

Timing Calibration and Windowing Technique Comparison for Lightning Mapping Arrays

B. M. Hare¹, H. Edens², P. Krehbiel², W. Rison², O. Scholten^{1,3}, S. Buitink^{4,5},
A. Corstanje^{4,5}, H. Falcke^{4,6,7}, J.R. Hörandel^{4,5,6}, T. Huege^{5,8}, G. K.
Krampah⁵, P. Mitra⁵, K. Mulrey⁵, A. Nelles^{9,10}, H. Pandya⁵, J. P. Rachen⁵, S.
Thoudam¹¹, T. N. G. Trinh¹², S. ter Veen^{4,7}, and T. Winchen¹³

¹Kapteyn Astronomical Institute, University of Groningen, P.O. Box 72, 9700 AB Groningen, Netherlands

²New Mexico Tech, 801 Leroy Place, Socorro, New Mexico 87801, USA

³Interuniversity Institute for High-Energy, Vrije Universiteit Brussel, Pleinlaan 2, 1050 Brussels, Belgium

⁴Department of Astrophysics/IMAPP, Radboud University Nijmegen, P.O. Box 9010, 6500 GL Nijmegen,
Netherlands

⁵Astrophysical Institute, Vrije Universiteit Brussel, Pleinlaan 2, 1050 Brussels, Belgium

⁶NIKHEF, Science Park Amsterdam, 1098 XG Amsterdam, Netherlands

⁷Netherlands Institute of Radio Astronomy (ASTRON), Postbus 2, 7990 AA Dwingeloo, Netherlands

⁸Institute for Astroparticle Physics (IAP), Karlsruhe Institute of Technology (KIT), P.O. Box 3640,

76021, Karlsruhe, Germany

⁹DESY, Platanenallee 6, 15738 Zeuthen, Germany

¹⁰ECAP, Friedrich-Alexander-University Erlangen-Nürnberg, 91058 Erlangen, Germany

¹¹Department of Physics, Khalifa University, PO Box 127788, Abu Dhabi, United Arab Emirates

¹²Department of Physics, School of Education, Can Tho University Campus II, 3/2 Street, Ninh Kieu

District, Can Tho City, Vietnam

¹³Max-Planck-Institut für Radioastronomie, P.O. Box 20 24, Bonn Germany

Key Points:

- The LOFAR telescope can be used to emulate and explore the operation of LMA networks
- Different, new, windowing techniques for LMAs are developed and compared
- A timing calibration technique for LMAs is developed and presented

Corresponding author: B. M. Hare, B.H.Hare@rug.nl

Corresponding author: W. Rison, rison@lmatechnologies.com

Abstract

Since their introduction 22 years ago, lightning mapping arrays (LMA) have played a central role in the investigation of lightning physics. Even in recent years with the proliferation of digital interferometers and the introduction of the LOw Frequency ARray (LOFAR) radio telescope, LMAs still play an important role in lightning science.

LMA networks use a simple windowing technique that records the highest pulse in either 80 μs or 10 μs fixed windows in order to apply a time-of-arrival location technique. In this work we develop an LMA-emulator that uses lightning data recorded by LOFAR to simulate an LMA, and we use it to test three new styles of pulse windowing. We show that they produce very similar results as the more traditional LMA windowing, implying that LMA lightning mapping results are relatively independent of windowing technique.

In addition, each LMA station has its own GPS-conditioned clock. While the timing accuracy of GPS receivers has improved significantly over the years, they still significantly limit the timing measurements of the LMA. Recently, new time-of-arrival techniques have been introduced that can be used to self-calibrate systematic offsets between different receiving stations. Applying this calibration technique to a set of data with 32 ns uncertainty, observed by the Colorado LMA, improves the timing uncertainty to 19 ns. This technique is not limited to LMAs and could be used to help calibrate future multi-station lightning interferometers.

1 Introduction

Since their introduction 22 years ago, lightning mapping arrays (LMAs) have played a central role in investigating lightning physics and storm electrification processes (Rison et al., 1999). Even in recent years with the proliferation of higher-time resolution digital interferometers (Stock et al., 2014) and the introduction of the LOw Frequency ARray (LOFAR) radio telescope (van Haarlem et al., 2013; B. M. Hare et al., 2018; B. Hare et al., 2019), LMAs still play an important role in lightning science due to being relatively easy to deploy, covering an area larger than an interferometer, and being able to detect lightning with significantly greater efficiency and detail than long-range lightning detection networks.

LMA networks use a simple windowing technique that records the highest pulse in fixed time windows, either 80 μs or 10 μs in length, in order to apply a time-of-arrival location technique. Such a windowing scheme could potentially be improved, as high-amplitude pulses that should be locatable often occur in the same time window, either at all or some of the stations, and/or with different peak amplitudes and being selected, in which case one or more pulses are not detected. This happens less often for 10 μs windows, but TOA data for the narrower windowing requires substantially longer times to process and is still affected to some extent by pulse overlap. Different windowing technique may produce different lightning images, potentially leading to different physics interpretations.

In this study we explore several different windowing techniques, and how they affect the imaged source locations. This study is conducted with an LMA-emulator that uses lightning data recorded by LOFAR to simulate an LMA. We compare the results of three new styles of windowing to traditional 80 μs LMA windowing for two lightning flashes. One of which is close to LOFAR, one of which is more distant. We also apply new time-of-arrival techniques for self-calibrating systematic offsets in LOFAR observations to develop an algorithm that corrects small remnant systematic timing differences between LMA stations. This algorithm is able to improve the timing accuracy of a set of data collected by the Colorado LMA (COLMA) (which typically has 25 ns uncertainty)

77 from 32 ns to 19 ns. This technique is very instrument-agnostic, and could be applied
78 to future multi-station interferometers.

79 2 Lightning Mapping Arrays

80 A lightning mapping array generally consists of 8 to 16 or more stations, and ac-
81 curately measures the arrival times of impulsive VHF radiation events. The signals are
82 received in a 6 MHz bandwidth in a locally unused television channel, with the arrival
83 times and window boundaries for each second derived from the 1 pps (pulse per second)
84 signals of a GPS receiver. The logarithmically-detected signals are digitized at a 25 MHz
85 rate with 16 bit precision and processed in an on-board field programmable gate array
86 (FPGA) to determine the peak event in successive 80- or 10 μ s time windows. Peak val-
87 ues above a floating noise threshold are saved to an output file. A subset of the data stream
88 is decimated to 400 μ s intervals and communicated via cellular data links to a central
89 computer for real-time processing and display. The full 80 μ s data is post-processed ei-
90 ther daily or as needed depending on available cell data speeds. The times of the pro-
91 cessing windows are fixed to align with the start and end of a second, and all process-
92 ing is done on a second-by-second basis. The noise threshold floats such that there are
93 about 1000 pulses recorded in a 1 s period (Thomas et al., 2004).

94 The LMA detections have two main sources of timing uncertainty. First, each peak
95 value has a random uncertainty of 12 ns rms, due to the peak time values being quan-
96 tized to 40 ns time values by the digitizer. This quantization effect represents the min-
97 imum possible timing uncertainty of a network. The other uncertainty concerns the one
98 second time interval. In particular, there is a \simeq 10–20-ns uncertainty in the timing of the
99 GPS 1 pps pulses from the GPS receiver, and a random 0 to 40 ns delay until the time
100 of the next 25 MHz clock pulse that defines the start of the one second interval. The tim-
101 ing uncertainty changes from second to second, but is systematic for a given second and
102 is different for each station.

103 Each LMA source has a reduced chi-squared goodness of fit given by

$$\chi_{\nu}^2 = \frac{1}{N_a - 4} \sum_j \frac{(M_j - t_j)^2}{\sigma_{\epsilon}^2} \quad (1)$$

104 where the sum is over each participating station. N_a is number of stations, and $(N_a - 4)$
105 is the number of degrees of freedom ν in the solution. M_j is the modeled arrival time
106 at the j th antenna, determined from the distance of the source from the station in ques-
107 tion. t_j is the measured arrival time at station j , and σ_{ϵ} is the rms timing uncertainty
108 of the network, which can be estimated from the chi-square distributions of processed
109 data. For current networks the timing uncertainty is about 25 ns rms. For a given source,
110 its chi-squared fit can also be expressed as a RMS timing uncertainty, given by

$$RMS = \sigma_{\epsilon} \sqrt{\chi_{\nu}^2|_i}, \quad (2)$$

111 where $\chi_{\nu}^2|_i$ is the reduced chi-square value of the particular source in question.

112 Following the normal procedure for LMA networks, we use the distribution of re-
113 duced chi-square values to estimate the rms timing uncertainty σ_{ϵ} of different LMA data
114 sets. This is done by plotting the distribution of the χ_{ν}^2 for different degrees of freedom,
115 and adjusting σ_{ϵ} until agreement with the theoretical chi-square distribution is obtained.
116 The resulting σ_{ϵ} is then the timing uncertainty of the data set. Using this procedure,
117 the timing uncertainty of the Colorado Lightning Mapping Array (COLMA) data used
118 in this work is about 32 ns, where COLMA typically has a timing uncertainty around
119 25 ns.

3 LOFAR and the LMA-emulator

In order to investigate different windowing techniques, we use continuously recorded VHF observations of two lightning flashes collected by LOFAR to emulate an LMA. We refer to this as an LMA-emulator. The benefit of such an emulator is that LOFAR saves five seconds of time series data for each trigger. Thus, the pipeline that each LMA station applies to its data in an on-line fashion can be applied to the LOFAR data as an off-line process, allowing us easily explore different aspects of the LMA on-line processing, such as the windowing technique. In addition, LOFAR has random timing uncertainties better than 1 ns, and we have developed an algorithm to calibrate out systematic timing differences between LOFAR stations. The longest LOFAR baselines are comparable to that of an LMA, up to 100 km (van Haarlem et al., 2013; B. M. Hare et al., 2018; B. Hare et al., 2019).

The LOFAR LMA-emulator uses data from two lightning flashes, one from 2018 and 2019, shown in Figures 1 and 2 respectively. For each flash, the stations were chosen to be as spread-out as possible in order to best emulate the layout of an LMA. For each station, the data was band-pass filtered between 60-66 MHz using a simple block filter, and the Hilbert envelope was found in order to emulate the log-amplifier of the LMA (which outputs the logarithm of signal power from the LMA antenna). Then, for each 80 μ s window aligned with the start of the second, the time of the highest peak was found, truncated to the nearest 40 ns, and saved to a file if the amplitude is greater than a noise threshold. Since LOFAR only saves five seconds of data, it is impossible to emulate the LMAs' floating noise threshold, so instead noise thresholds were chosen visually. The times of the resulting pulses were then passed through the LMA processing algorithm. In Section 4 we test other windowing techniques to explore their effect. The LOFAR LMA-emulator has a timing uncertainty of about 15 ns, which is dominated by the quantization of source arrival time when converting the LOFAR data into the LMA data format. After processing, the best-located sources (located by all stations, with chi-squared values better than 1) have location errors in easting, northing, and altitude around 9 m, 21 m, 48 m, and 3 m, 2 m, and 20 m for the 2018 and 2019 flashes respectively. These location errors were calculated via the analytical covariance matrix.

4 Effect of Windowing on an LMA

In this section we use the LOFAR LMA-emulator to test the effect of different windowing techniques on LMA data and processing. First, we test the traditional binning technique with 80 μ s wide windows that align with the start of the second. Then we test three new windowing techniques that we will refer to as “non-aligned window”, “floating threshold”, and “natural threshold”. The details of these three windowing techniques are described below.

One challenge in this study was that the current LMA software implementation requires that there is only one recorded pulse per window (of either a 10 μ s or 80 μ s width), where the time of the window is fixed such that the windows align with the start and end of each second. Our new windowing techniques, however, must record multiple pulses per second-aligned window, or else the result will be equivalent to the traditional windowing. To solve this we have designed our new windowing techniques to try to match the same average pulse rate of the traditional 80 μ s window (that is, an average of 1 recorded pulse per 80 μ s), but not have more than one recorded pulse per second-aligned 10 μ s window. We then processed all the data with the 10 μ s mode of the LMA processing algorithm, including the traditional 80 μ s window for consistency.

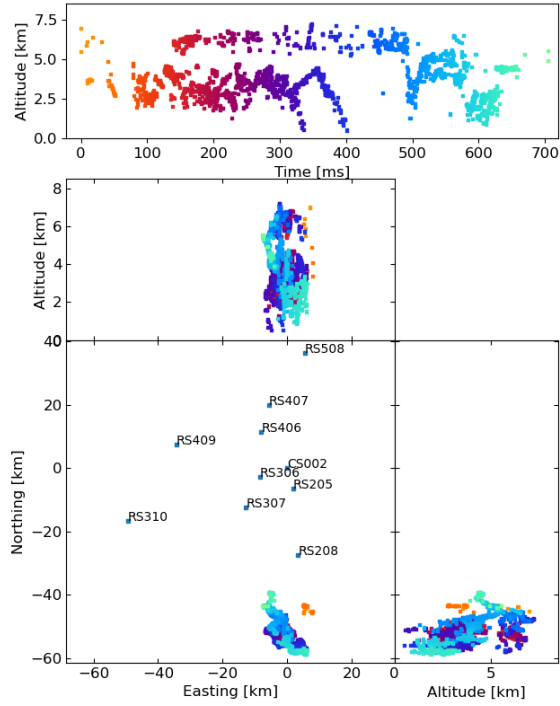


Figure 1. The 2018 lightning flash mapped by the LOFAR LMA emulator using the traditional LMA windowing technique, along with the used LOFAR stations. Showing sources that have 8 or more participating stations and a chi-squared value better than 2 (RMS < 21 ns).

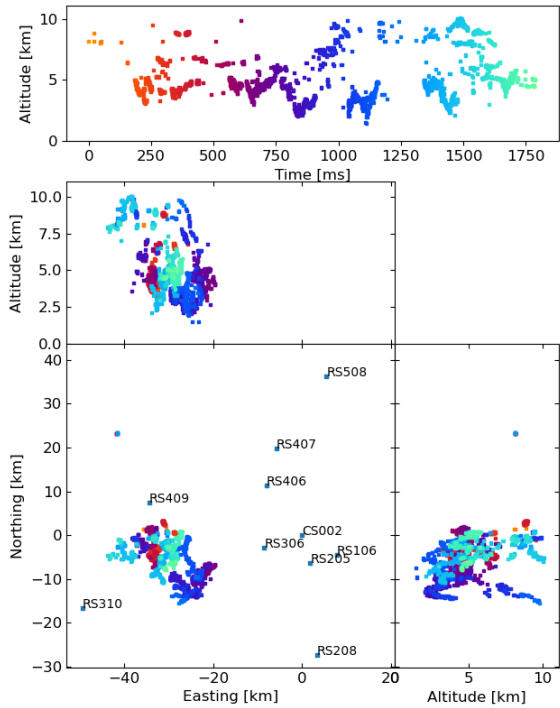


Figure 2. The 2019 lightning flash mapped by the LOFAR LMA emulator using the traditional LMA windowing technique, along with the used LOFAR stations. Showing sources that have 8 or more participating stations and a chi-squared value better than 2 (RMS < 21 ns).

167

4.1 Non-Aligned Window

168

169

170

171

172

173

174

175

176

177

178

179

180

181

182

The first new windowing technique is rather simple. A sample is recorded as a pulse if it has the highest amplitude within a $\pm 40 \mu\text{s}$ region. Note that these windows can overlap, so two recorded pulses can be as close as $40 \mu\text{s}$. We choose to test this method because the traditional windowing technique has a minimum time between pulses that varies randomly. This is because the times of the windows are fixed to be aligned with the start of the second as opposed to the time of the recorded pulse. Thus, since the recorded pulse can occur anywhere in a window, and the next recorded pulse can only occur as early as the start of the next window, than the minimum time between pulses is uniformly random from 0 up to the window width. This non-aligned windowing technique, however, fixes the minimum time between pulses to be exactly $40 \mu\text{s}$. The hope is that this improved consistency will allow the windowing technique to more reliably pick pulses that correspond with each other between the different stations. We expect, and show below, that a $40 \mu\text{s}$ minimum time, as opposed to a $80 \mu\text{s}$, will result in about the same number of pulses as the traditional windowing. As the traditional windowing has an average minimum time of $40 \mu\text{s}$ (as it is uniformly distributed between 0 to $80 \mu\text{s}$).

183

4.2 Floating Threshold

184

185

186

187

188

The goal of the second new windowing technique is to improve the ability of the LMA to handle bursts of pulses. That is, to allow the windowing technique to record pulses that are close together in time, but to have an amplitude threshold so that the average rate of pulses is similar to the traditional $80 \mu\text{s}$ windowing (an average of 1 recorded pulse per $80 \mu\text{s}$).

189

190

191

192

193

194

195

196

197

198

199

This is done by implementing a floating threshold similar to the floating noise threshold already present in LMAs, but shortened to work on a smaller timescale. To do this, we track the highest sample in $10 \mu\text{s}$ bins, similar to the traditional $10 \mu\text{s}$ windowing. However, this sample is only recorded to file if its amplitude is larger than a threshold that is adjusted every $400 \mu\text{s}$. If there are more than five recorded pulses in the previous $400 \mu\text{s}$ then the threshold is increased by ten percent, if there are less than five then the threshold is decreased by ten percent. Note that each $400 \mu\text{s}$ period is consecutive and not overlapping, because if the periods overlap then this technique will become unstable and the threshold will oscillate up and down even when the pulse amplitude distribution in the data is constant. A noise threshold is still implemented, and any pulse that has an amplitude below the noise threshold is discarded.

200

4.3 Natural Threshold

201

202

203

204

205

206

207

208

Our final windowing technique has a similar goal to the floating threshold, in that we want to be able to record pulses that occur close-together in time while maintaining an average rate of $80 \mu\text{s}$, which we accomplish with a dynamic amplitude threshold. The difference between this technique and the floating threshold, is that this technique has the additional goal that we do not want to explicitly track this amplitude threshold. Instead, we want a simple technique that only considers data centered on each pulse completely independently, not relying on memory of which pulses were previously recorded to file.

209

210

211

212

213

214

215

We have accomplished this by first finding the highest sample in $10 \mu\text{s}$ bins, again like the traditional LMA windowing, but we do not record this pulse. Instead we save it into a circular buffer of $80 \times 10 \mu\text{s}$ bins (a total width of $800 \mu\text{s}$). The sample in the 40th bin (that is the sample in the middle of our buffer) is recorded to file if no more than 9 other bins contain stronger pulses. i.e., a pulse is saved to file if it is the one of the top 10 strongest pulses in $800 \mu\text{s}$ (centered on that pulse) and it is above the noise threshold. This results in an average of 10 pulses recorded per $800 \mu\text{s}$, and the decision of whether

216 or not a pulse is recorded is entirely independent of whether or not any other pulse is
 217 saved.

218 This natural threshold windowing technique has one potential drawback over the
 219 traditional 80 μ s windowing technique. This is due to the possibility that a lightning pro-
 220 cess could produce a very strong VHF burst that lasted around 100 μ s long. If this oc-
 221 curred, then the natural threshold window would saturate on just that VHF burst and
 222 would not record any other VHF emissions for ± 400 μ s centered around that burst. The
 223 traditional 80 μ s windowing technique does not present this problem.

224 4.4 Results

225 Figures 3, 4, 5, and 6 show results for the four windowing techniques for the 2018
 226 flash, zoomed in to a well-imaged negative leader. Sources with 8 or more participating
 227 stations are shown. Figures 7, 8, 9 and 10 are similar for the 2019 flash.

228 Some statistical results for each windowing technique are shown in Tables 1 and
 229 2 for the 2018 and 2019 flashes respectively. The row “average pulses per station” gives
 230 the number of pulses recorded with the relevant method averaged over all ten LOFAR
 231 stations, over the absolute theoretical maximum number of pulses that could have been
 232 recorded. Row “relative pulse number difference” gives the difference between the min-
 233 imum and maximum number of pulses recorded for each station, divided by the aver-
 234 age recorded pulses per station, in order to give a measure of the deviation of recorded
 235 pulses between stations. As one would expect, stations farther from the flash recorded
 236 fewer pulses. Next there are four sets of two rows. These are two statistics for four dif-
 237 ferent cuts of sources. The four sets of cuts are: 1) no cuts (all sources output by the
 238 LMA processing algorithm), 2) sources that have 8 or more participating stations, 3) sources
 239 that pass cut 2 and have a chi-squared value less than 2 (RMS < 21 ns), finally 4) sources
 240 that pass cut 3 and are in the vicinity of the imaged flash. For each of the four cuts we
 241 list the number of sources, and the ratio between number of sources and the number of
 242 recorded pulses.

243 As discussed in Section 2, the timing uncertainty of an LMA dataset can be found
 244 by matching the calculated reduced chi-square distribution with the expected reduced
 245 chi-square distribution. Doing so we found that the timing uncertainty for all four win-
 246 dowing techniques was 14 ns. In other words, the windowing technique does not seem
 247 to affect the timing uncertainty for our LMA-emulator. The 14 ns uncertainty is essen-
 248 tially the quantization uncertainty of 25 MHz digitization discussed in Sections in 2 and
 249 3.

250 From these results we can see that the four windowing techniques produce simi-
 251 lar results. A comparison between the images shown in Figures 3, 5, 6, and 4 for the 2018
 252 flash and Figures 7, 9, 10, and 8 for the 2019 flash show that each of the windowing tech-
 253 niques shows the same general features on the 100 m scale.

254 Table 1 shows that, for the 2018 flash, the non-aligned windows gives a nearly iden-
 255 tical result to the traditional LMA windowing. The natural threshold, on the other hand,
 256 has a slightly improved ($\approx 10\%$) ratio between located events over received pulses. The
 257 floating threshold saved significantly more pulses than the other windowing techniques,
 258 despite being designed to have the same rate. The reason for recording more pulses than
 259 intended is because the amplitude distribution of pulses in a lightning flash can change
 260 very quickly, which makes it very difficult to design a floating threshold that behaves pre-
 261 dictably. Table 2 shows very similar results for the 2019 flash. It also shows that every
 262 windowing technique had significantly lower ratios between located sources and detected
 263 pulses during the 2019 flash as compared to the 2018 flash. It is presently unknown why
 264 different flashes result in different processing efficiencies.

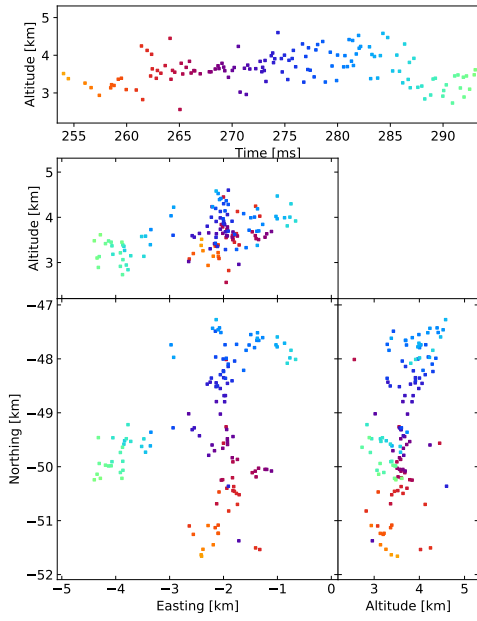


Figure 3. $80 \mu\text{s}$ traditional windowing with the LMA-emulator, centered on a negative leader in the 2018 flash. Showing 134 sources that have 8 or more participating stations.

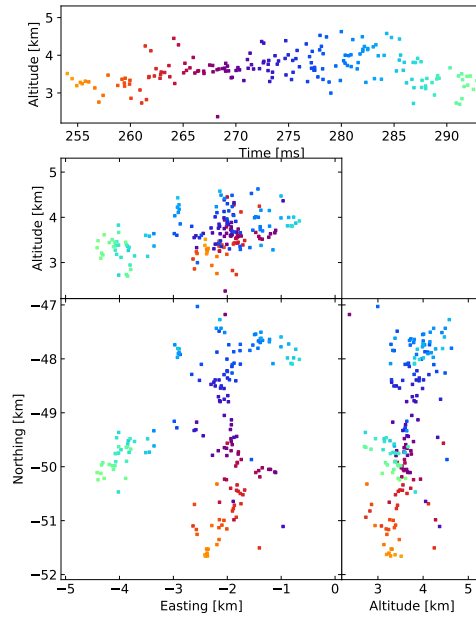


Figure 4. Natural threshold windowing with the LMA-emulator, centered on a negative leader in the 2018 flash. Showing 181 sources that have 8 or more participating stations.

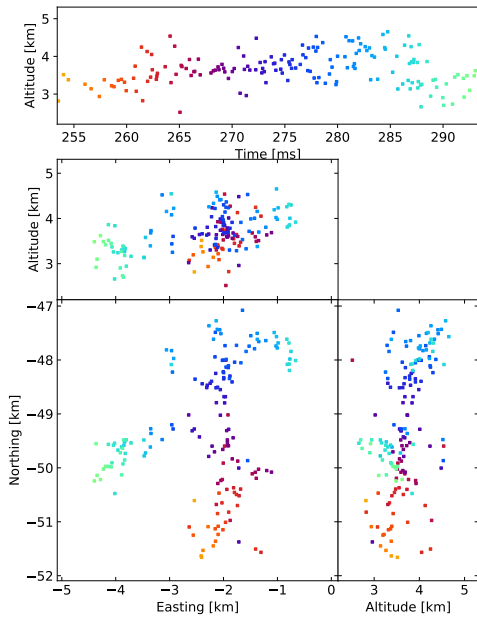


Figure 5. Non-aligned windowing with the LMA-emulator, centered on a negative leader in the 2018 flash. Showing 164 sources that have 8 or more participating stations.

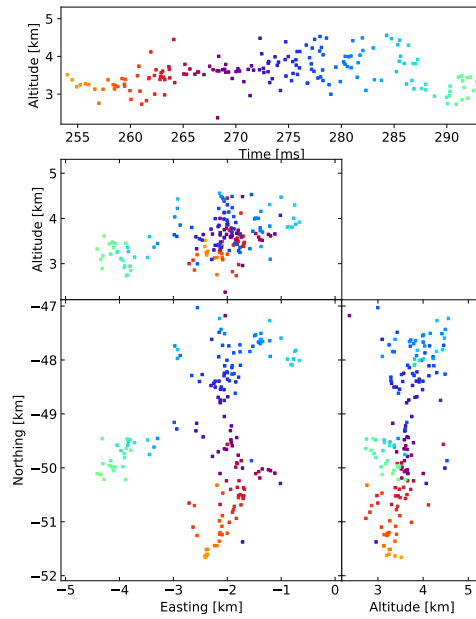


Figure 6. Floating threshold windowing with the LMA-emulator, centered on a negative leader in the 2018 flash. Showing 173 sources that have 8 or more participating stations.

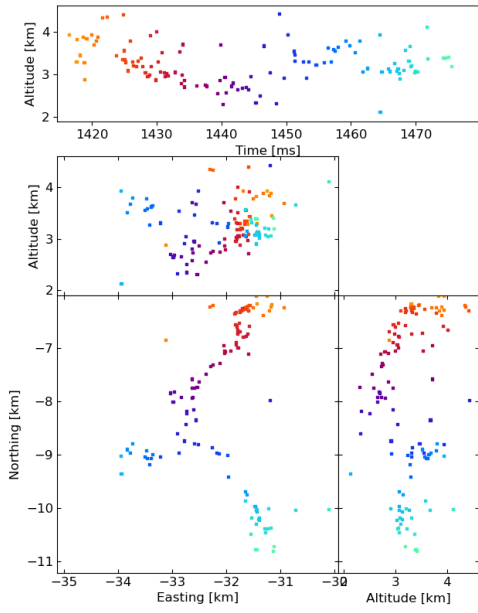


Figure 7. $80 \mu\text{s}$ traditional windowing with the LMA-emulator, centered on a negative leader in the 2019 flash. Showing 117 sources that have 8 or more participating stations.

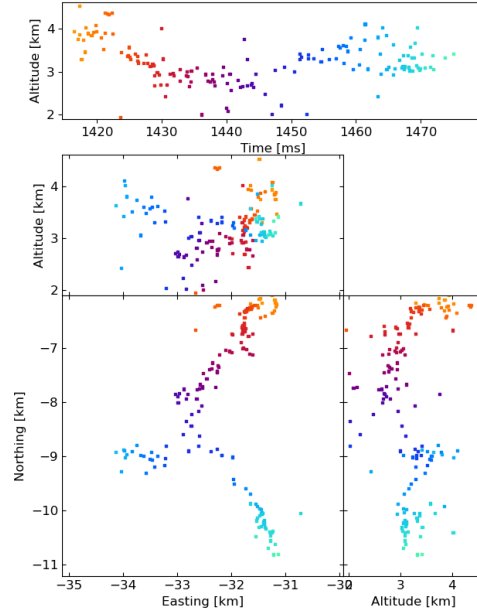


Figure 8. Natural threshold windowing with the LMA-emulator, centered on a negative leader in the 2019 flash. Showing 152 sources that have 8 or more participating stations.

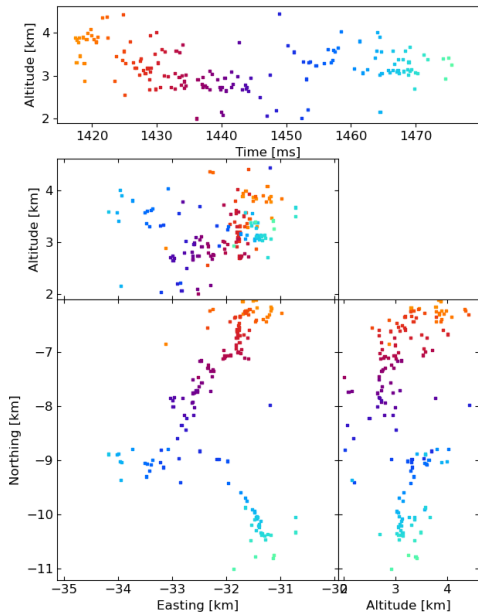


Figure 9. Non-aligned windowing with the LMA-emulator, centered on a negative leader in the 2019 flash. Showing 154 sources that have 8 or more participating stations.

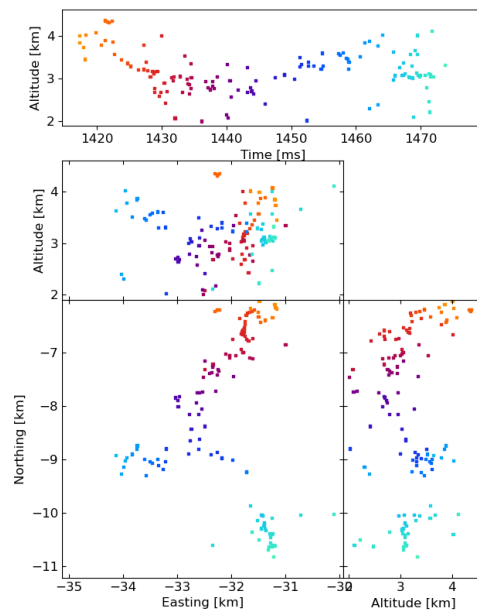


Figure 10. Floating threshold windowing with the LMA-emulator, centered on a negative leader in the 2019 flash. Showing 130 sources that have 8 or more participating stations.

Table 1. Results of different windowing techniques for the 2018 flash.

Statistic	80 μ s windows	non-aligned windows	floating threshold	natural threshold
average recorded pulses / maximum pulses	6,450 / 8,800	6,340 / 8,800	9,032 / 70,500	6,944 / 70,500
relative pulse number difference	0.50	0.48	0.62	0.39
number sources (no cut)	4,120	4,592	7,552	5,222
source/pulse ratio	0.64	0.72	0.84	0.75
number sources (Cut 1)	1,905	2,257	2,796	2,729
source/pulse ratio	0.29	0.35	0.31	0.39
number sources (Cut 2)	1,489	1,749	2,078	2,092
source/pulse ratio	0.23	0.27	0.23	0.30
number sources (Cut 3)	1,466	1,722	2,044	2,059
source/pulse ratio	0.23	0.27	0.23	0.30

Table 2. Results of different windowing techniques for the 2019 flash.

Statistic	80 μ s windows	non-aligned windows	floating threshold	natural threshold
average recorded pulses / maximum pulses	13,180 / 22,500	12,730 / 22,500	21,860 / 180,200	14,260 / 180,200
relative pulse number difference	0.38	0.36	0.62	0.32
number sources (no cut)	8,123	9,011	20,700	11,030
source/pulse ratio	0.62	0.70	0.95	0.77
number sources (Cut 1)	3,226	3,997	3,561	4,006
source/pulse ratio	0.24	0.31	0.16	0.28
number sources (Cut 2)	1,687	2,053	1,890	2,121
source/pulse ratio	0.13	0.16	0.09	0.15
number sources (Cut 3)	1,675	2,041	1,879	2,109
source/pulse ratio	0.13	0.16	0.09	0.15

265 Table 1 shows that, for the 2018 flash, the non-aligned windows records slightly less
 266 pulses than the traditional LMA windowing, but results in slightly more located events.
 267 The natural threshold saved about 8% more pulses, but was able to located about 40%
 268 more events. The floating threshold saved significantly more pulses than the other win-
 269 dowing techniques, despite being designed to have the same rate. The reason for record-
 270 ing more pulses than intended is because the amplitude distribution of pulses in a light-
 271 ning flash can change very quickly, which makes it very difficult to design a floating thresh-
 272 old that behaves predictably. Table 2 shows very similar results for the 2019 flash. It also
 273 shows that every windowing technique had significantly lower ratios between located sources
 274 and detected pulses during the 2019 flash as compared to the 2018 flash. It is presently
 275 unknown why different flashes result in different processing efficiencies.

276 It is interesting to compare the distributions of time between recorded pulses for
 277 each of the four windowing techniques. This is shown in Figures 11, 12, 13, 14 for the
 278 2019 flash. These figures also show a straight line, which is the expected distribution if
 279 pulses were recorded with a random independent rate of 1 per 80 μ s. The same distri-
 280 butions for the 2018 flash look extremely similar. As one would expect, the distribution
 281 of times between recorded pulses for traditional binning, shown in Figure 11, has a sym-
 282 metrical peak around 80 μ s with a tail extending to longer time scales. The natural thresh-
 283 old, shown in figure 12 has an extremely good match to an independent random rate,
 284 as designed. However, it has a spike at time-differences of 10 μ s, which could be due to
 285 the fact that this technique still uses 10 μ s binning at its core to operate. Non-aligned
 286 binning, shown in figure 13, is similar to the traditional windowing, except that there
 287 are no pulses closer than 40 μ s and the distribution has a smoother transition between
 288 the central peak and tail (starting at about 160 μ s). Finally, the distribution produced
 289 by the floating threshold is shown in figure 14, which has a very strong peak at around
 290 10 μ s, followed by a fairly regular rate that is lower than 1 per 80 μ s.

291 5 Timing Calibration

292 In this section we apply the calibration technique that we developed for LOFAR,
 293 to the LMA data. This calibration technique is capable of finding any relative timing
 294 offset between LMA stations, including the GPS timing offsets.

295 5.1 The Algorithm

296 The fundamental idea behind our calibration algorithm is that the time between
 297 pulses of different sources on each antenna, even if the absolute time is unknown, is enough
 298 to constrain the source location. This information is used simply by fitting the arrival
 299 times of pulses from multiple sources, where the fitting parameters are the location and
 300 time of each source and the relative timing offset of all but one station. This is expressed
 301 through Equations 3 and 4, where Equation 3 is the modeled arrival time given the source
 302 locations and relative station delays, and Equation 4 is the reduced chi-squared.

$$M_{i,j} = \frac{\sqrt{(x_i - x_j)^2 + (y_i - y_j)^2 + (z_i - z_j)^2}}{C} + t_i + \Delta t_j \quad (3)$$

303 where $M_{i,j}$ is the calculated arrival time for the i th source on the j th antenna. $x_i, y_i,$
 304 $z_i,$ and t_i is the location and time of the i th source. $x_j, y_j, z_j,$ and Δt_j is the location
 305 and time delay of j th antenna. C is the speed of light. The fitted parameters are $x_i, y_i,$
 306 $z_i, t_i,$ and $\Delta t_j,$ which are the locations and times of the sources, and the time delays of
 307 the antennas. Note that the time delay for one station, the reference station, is held to
 308 0. Given this point source model, the reduced chi-squared can be calculated,

$$\chi^2(x_i, y_i, z_i, t_i, \Delta t_j) = \frac{1}{N_m - N_a - 4N_s} \sum_{i,j} \frac{(M_{i,j} - t_{i,j})^2}{\sigma_\epsilon^2} \quad (4)$$

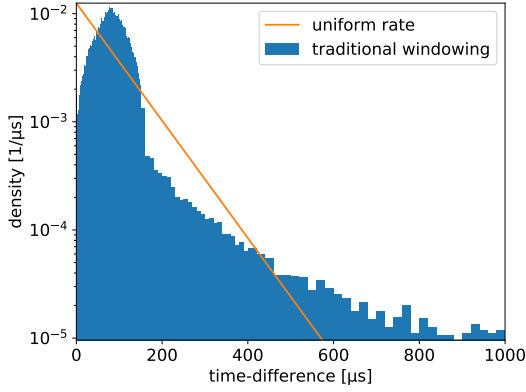


Figure 11. Distribution of time between saved pulses for the traditional $80 \mu\text{s}$ windowing technique. The line shows the expected distribution if the pulses were saved at a random rate of 1 per $80 \mu\text{s}$.

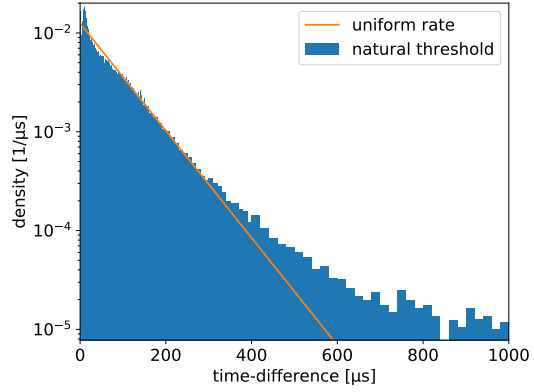


Figure 12. Distribution of time between saved pulses for the natural threshold windowing technique. The line shows the expected distribution if the pulses were saved at a random rate of 1 per $80 \mu\text{s}$.

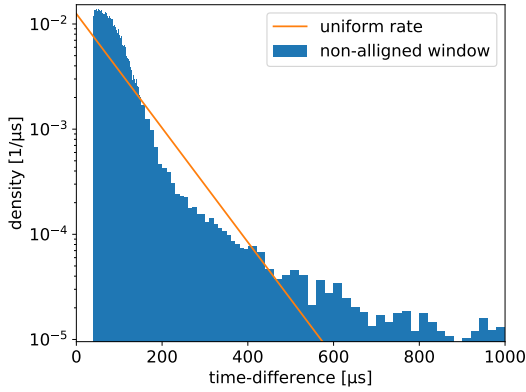


Figure 13. Distribution of time between saved pulses for the non-aligned windowing technique. The line shows the expected distribution if the pulses were saved at a random rate of 1 per $80 \mu\text{s}$.

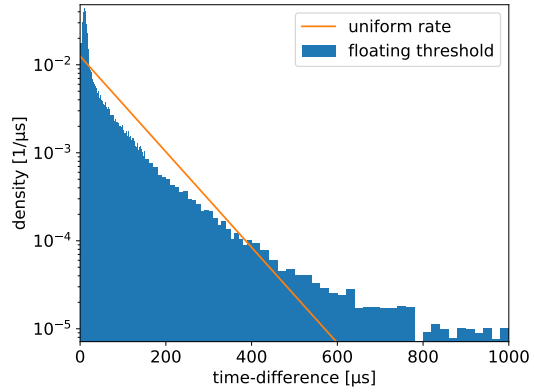


Figure 14. Distribution of time between saved pulses for the floating threshold windowing technique. The line shows the expected distribution if the pulses were saved at a random rate of 1 per $80 \mu\text{s}$.

309 where χ^2 is the reduced the chi-squared. N_m is the number of measurements, that is,
 310 the sum of number of active antennas used in locating each source. N_s is the number
 311 of sources fitted. N_a is the number of antennas. $t_{i,j}$ is the measured arrival time of source
 312 i on antenna j . Note this sum skips i,j combinations when the i th source is not detected
 313 on the j th antenna. The decision of which pulse to use in locating an event, and whether
 314 or not to exclude a station entirely is made by the LMA processing algorithm. Finally,
 315 σ_ϵ is the estimated timing uncertainty.

316 The difference between this technique and normal LMA source locating is that mul-
 317 tiple sources are fit simultaneously, and the relative time calibrations between stations
 318 are fitted parameters.

319 The difficulty in any time-of-arrival algorithm is deciding which measured pulse times
 320 to associate with which source. For the LMA this problem already has a solution in the
 321 LMA data processing program. This program, fortunately, also saves the times of the
 322 pulses associated with each source accounting for known delays. Thus, our algorithm is
 323 designed to be applied to processed LMA data. The resulting delays can then be fed back
 324 into the LMA processing code in order to produce a better image. However, since the
 325 LMAs' systematic timing delays change at the beginning of every second, via the GPS
 326 updating the station clock, our algorithm has to be applied separately to each second
 327 of LMA data.

328 Each calibration run uses between 20-50 LMA sources and their associated pulses
 329 to find the locations, times, and antenna delays that minimize the χ^2 value, via a Levenberg-
 330 Marquardt minimizer. In order to estimate the uncertainty of the extracted relative tim-
 331 ing delays, this procedure is run multiple times on different sets of sources. We sort the
 332 LMA sources so that, for the number of runs (N_r) there are at least N_p sources on each
 333 antenna. The extracted delays are then the average of the runs, and the estimated un-
 334 certainties are the standard deviation of the runs divided by the square root of number
 335 of runs. The LMA sources used in the calibration were chosen by picking LMA sources
 336 at random that have RMS fit values better than the timing uncertainty of the LMA net-
 337 work, and a minimal number of participating stations. We purposefully do not pick LMA
 338 sources with the absolute best fit values, as they tend to have random uncertainty that
 339 cancel-out the systematic uncertainties that we wish to extract. The full procedure is
 340 shown in Algorithm 1.

Algorithm 1: Algorithm to extract station delays

Result: relative timing delays and estimated uncertainties
 Sort LMA sources in N_r groups, with at least N_p sources per antenna in each
 group;
 Choose reference station;
for $run \leftarrow 1$ **to** N_r **do**
 341 | extract source locations and station delays by minimizing equation 4;
 | throw away extracted source locations;
 | store station delays;
end
 delay for each station is the average;
 estimated uncertainty is the standard deviation divided by square root of N_r ;

342 5.2 Calibration Test with the LOFAR LMA-Emulator

343 The LOFAR LMA-Emulator presents a perfect platform for which to test our cal-
 344 ibration algorithm, since the LOFAR data has already been calibrated such that any sys-
 345 tematic uncertainty (~ 1 ns) is much smaller than the random uncertainty inherent in
 346 the LMA emulator (~ 12 ns). In order to perform this test we ran the LOFAR LMA-
 347 emulator to obtain a set of LMA sources based on lightning data recorded by LOFAR.

Table 3. Results of applying the calibration algorithm to the LMA-emulator. CS002 was the reference station.

station	injected delay [ns]	extracted delay [ns]	estimated uncertainty [ns]	actual error [ns]
CS002	0.0	0.0	0.0	0.0
RS205	-1.6	0.0	1.0	-1.6
RS306	-7.1	-7.0	0.8	-0.1
RS406	-11.9	-15.2	0.9	3.3
RS307	17.2	18.5	1.2	-1.3
RS407	7.7	7.9	1.5	-0.2
RS409	-10.6	-11.4	0.8	0.8
RS208	-20.0	-20.4	0.9	0.4
RS508	6.6	7.6	0.9	-1.0
RS310	-8.9	-8.3	0.6	-0.6

348 We then injected a systematic delay to the pulses recorded by each station. These in-
349 jected systematic delays were drawn independently from a normal distribution with 10 ns
350 standard deviation. We then ran our calibration technique, algorithm 1, and attempted
351 to re-extract the injected delays with expected uncertainties. Note that this test injects
352 the systematic timing uncertainty after the LMA location algorithm, where, in reality,
353 the systematic timing uncertainties are injected before the LMA location algorithm. The
354 implication is, in a more realistic situation the offsets we wish to find could cause the
355 LMA location algorithm to associate the wrong pulse with an event. Thus, since we rely
356 on the LMA location algorithm to pick which pulses to associate with each event, real
357 data could result in a somewhat lower quality calibration than indicated by this test.

358 The injected delays, extracted delays, estimated uncertainties and actual uncertain-
359 ties are shown in Table 3. Note that, despite using ten stations, only nine are shown in
360 Table3 since both the injected and estimated uncertainty were held to zero on the ref-
361 erence station, which was CS002.

362 Table 3 shows that the extracted time delays are very similar to the injected time
363 delay, and that the estimated uncertainties in general reflect the actual uncertainties. In
364 this particular run there is one station, RS406, where the difference between the extracted
365 delay and injected delay is 3 to 4 times that of the estimated uncertainty. This, however,
366 is not surprising, as the estimated uncertainty is probably only accurate to a factor of
367 2.

368 5.3 Application of Calibration to COLMA

369 We have applied our new calibration algorithm to 600 seconds of data from the Col-
370 orado Lightning Mapping array. We found that the timing uncertainty improved from
371 32 ns to 19 ns. This represents a significant improvement, however, it is known that the
372 random uncertainty the LMA should be around 12 ns. Indeed, the LOFAR LMA-emulator,
373 which attempts to emulate the dominant random uncertainty sources of the LMA, has
374 a timing uncertainty of about 15 ns. Thus, we'd expect the post-calibration timing un-
375 certainty to be better than 19 ns, and it is not clear why this is not the case. One pos-
376 sibility is that the calibration algorithm used poorly reconstructed LMA sources, where
377 pulses from different real VHF sources were associated with each-other, which could have
378 biased the result.

379 Each of these 600 seconds were processed independently, and since the timing of
380 the LMA stations is updated every second the resulting timing calibrations will be dif-

Table 4. Average, standard deviation, and standard error of the mean from applying the calibration procedure to COLMA data, where Rodenburg was the reference station.

COLMA station	average delay [ns]	delay standard deviation [ns]	uncertainty of the average [ns]
Rodenburg	0.0	0.0	0.0
Briggsdale	-21.2	32.0	4.2
LoneTree	-6.5	55.3	7.3
GreeleyArpt	-12.1	18.0	2.4
Raymer	33.3	57.1	7.5
FtCollinsArpt	-1.8	25.0	3.3
Herford	-9.5	62.3	8.1
Homestead	-18.3	61.3	8.0
Purcell	4.7	37.4	4.8
CPER	-22.0	46.0	6.0
WeldCHS	3.0	17.1	2.2
ButteEdge	5.3	54.0	7.1
Boyer	-0.1	43.8	5.8
FMA	-15.8	35.2	4.6
WigginsHS	8.1	31.5	4.2

381 ferent for every second according to the timing error of the LMA. In order to explore this
382 second-to-second calibration variation, Table 4 reports the average extracted delay which
383 should be zero (within statistical fluctuations) if each station has no unaccounted sys-
384 tematic timing delay. The second column of Table 4 shows the standard deviation of the
385 extracted delay, which is due to (and should be similar to) the LMA timing error (32 ns).
386 These standard deviations do not reflect the accuracy of the calibrations. The final col-
387 umn gives the estimated uncertainty of the average (calculated through standard devi-
388 ation divided by square root of number of samples). Since every processed second can
389 use a different reference station, we only used extracted delays that had the same ref-
390 erence station (Rodenburg) in order to calculate the statistics in Table 4. Out of the 600 s
391 of processed LMA data, our algorithm used the Rodenburg station for 58 of the processed
392 seconds. Therefore 58 samples were used to derive the statistics shown in Table 4.

393 The standard deviations are about 32 ns, which is consistent with the known tim-
394 ing error of this set of COLMA data. A few stations have large average delays (greater
395 than three times the uncertainty). This implies that the COLMA LMA has significant
396 un-accounted-for systematic relative delays other than GPS-related timing offsets. The
397 source of these systematic relative delays is not clear, as all COLMA stations use the same
398 cable lengths in order to minimize this exact problem. More work would be needed to
399 explore if this is indeed the case, and what the cause of these systematic offsets could
400 be.

401 Figure 15 and 16 shows a negative leader imaged by COLMA before and after cal-
402 ibration respectively. These figures show 280 and 286 sources that have 8 or more par-
403 ticipating stations respectively. These figures show that, despite the significant improve-
404 ment in timing, there is little improvement in image quality as the two images are ex-
405 tremely similar.

406 6 Conclusion

407 In this work we developed a system to emulate the operation of a LMA with LO-
408 FAR. This LMA-emulator allowed us to test the effect of different windowing techniques.

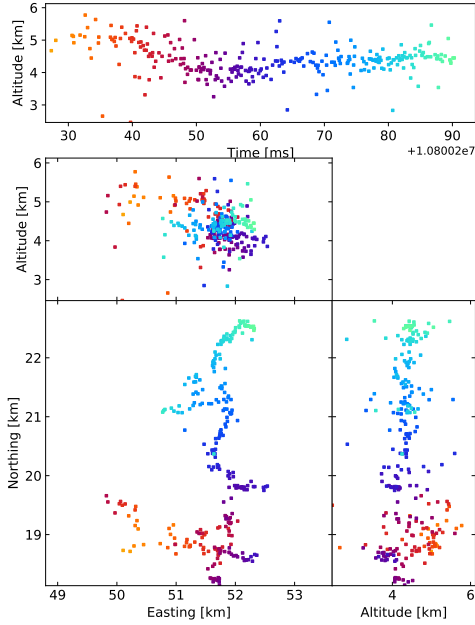


Figure 15. Negative leader imaged by COLMA before calibration. 280 sources with 8 or more participating stations are shown.

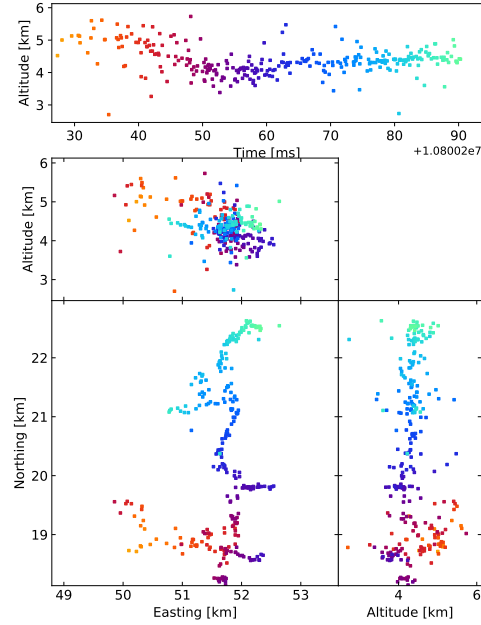


Figure 16. Negative leader imaged by COLMA after calibration. 286 sources with 8 or more participating stations are shown.

409 We tested three new windowing techniques and compared them to the traditional LMA
 410 windowing. We found that these more sophisticated windowing techniques result in im-
 411 ages that are, by eye, not obviously improved over the older simpler technique. This shows
 412 that lightning physics extracted using LMAs is not sensitive to the windowing technique
 413 used.

414 In addition, we have developed a new calibration technique, based on our experi-
 415 ence with calibrating LOFAR, that can extract relative systematic timing delays between
 416 LMA stations on a second-by-second basis. Using this calibration technique we were able
 417 to reduce the timing uncertainty of 600 seconds of data collected from COLMA from 32 ns
 418 to 19 ns, when COLMAs' typical timing uncertainty is about 25 ns.

419 Despite the modest improvements of these techniques to the LMA data, we believe
 420 that this work has three important implications. Firstly, by demonstrating the unique
 421 flexibility of the LOFAR instrument. At the moment LOFAR is operated in a triggered
 422 mode, to produce high-quality images of a few flashes (e.g. (B. Hare et al., 2019; Scholten
 423 et al., 2021)). However, this work suggests the possibility of operating LOFAR in a con-
 424 tinuous LMA-like mode to capture every lightning flash in a storm with lower quality,
 425 which will be investigated in future work. Secondly, this work testifies to the robustness
 426 of the LMA system and processing algorithm, that even significant changes to the pro-
 427 cessing technique do not result in noticeable differences in the reconstructed lightning.
 428 Finally, and perhaps most critically, this work establishes two new post-processing tech-
 429 niques that can be applied to almost any lightning-mapping system, not just LMAs. This
 430 is especially important for multi-station lightning interferometers, which have proven to
 431 be very difficult to calibrate without this technique (B. M. Hare et al., 2018; Jensen et
 432 al., n.d.).

433 **Acknowledgments**

434 The LOFAR cosmic-ray key science project acknowledges funding from an Advanced
 435 Grant of the European Research Council (FP/2007-2013) / ERC Grant Agreement n.
 436 227610. The project has also received funding from the European Research Council (ERC)
 437 under the European Union’s Horizon 2020 research and innovation programme (grant
 438 agreement No 640130). We furthermore acknowledge financial support from FOM, (FOM-
 439 project 12PR304). ST acknowledges funding from the Khalifa University Startup grant
 440 (project code 8474000237). BMH is supported by NWO (VI.VENI.192.071). KM is sup-
 441 ported by FWO (FWOTM944). AN acknowledges the DFG grant NE 2031/2-1. TNGT
 442 acknowledges funding from the Vietnam National Foundation for Science and Technol-
 443 ogy Development (NAFOSTED) under [Grant number 103.01-2019.378]. LOFAR, the
 444 Low Frequency Array designed and constructed by ASTRON, has facilities in several coun-
 445 tries, that are owned by various parties (each with their own funding sources), and that
 446 are collectively operated by the International LOFAR Telescope foundation under a joint
 447 scientific policy.

448 The data used in this work is available at (B. Hare et al., 2020).

449 **References**

- 450 Hare, B., Edens, H., Krehbiel, P., Rison, W., Scholten, O., Buitink, S., . . . Winchen,
 451 T. (2020). *processed data for “Timing Calibration and Windowing Technique*
 452 *Comparison for Lightning Mapping Arrays”*. DataverseNL. Retrieved from
 453 <https://doi.org/10.34894/QY56WJ> doi: 10.34894/QY56WJ
- 454 Hare, B., et al. (2019). Needle-like structures discovered on positively charged light-
 455 ning branches. *Nature*, *568*, 360–363. doi: 10.1038/s41586-019-1086-6
- 456 Hare, B. M., et al. (2018). LOFAR Lightning Imaging: Mapping Lightning With
 457 Nanosecond Precision. *Journal of Geophysical Research: Atmospheres*, *123*(5),
 458 2861-2876. doi: 10.1002/2017JD028132
- 459 Jensen, D. P., Sonnenfeld, R. G., Stanley, M. A., Edens, H. E., da Silva, C. L., &
 460 Krehbiel, P. R. (n.d.). Dart-leader and k-leader velocity from initiation site to
 461 termination time-resolved with 3d interferometry. *Journal of Geophysical Re-*
 462 *search: Atmospheres*, *n/a*(n/a), e2020JD034309. Retrieved from [https://](https://agupubs.onlinelibrary.wiley.com/doi/abs/10.1029/2020JD034309)
 463 agupubs.onlinelibrary.wiley.com/doi/abs/10.1029/2020JD034309
 464 (e2020JD034309 2020JD034309) doi: <https://doi.org/10.1029/2020JD034309>
- 465 Rison, W., Thomas, R. J., Krehbiel, P. R., Hamlin, T., & Harlin, J. (1999). A
 466 gps-based three-dimensional lightning mapping system: Initial observations in
 467 central new mexico. *Geophysical Research Letters*, *26*(23), 3573-3576. doi:
 468 10.1029/1999GL010856
- 469 Scholten, O., Hare, B. M., Dwyer, J., Sterpka, C., Kolmašová, I., Santolík, O.,
 470 . . . Winchen, T. (2021). The initial stage of cloud lightning imaged in
 471 high-resolution. *Journal of Geophysical Research: Atmospheres*, *126*(4),
 472 e2020JD033126. Retrieved from [https://agupubs.onlinelibrary.wiley](https://agupubs.onlinelibrary.wiley.com/doi/abs/10.1029/2020JD033126)
 473 [.com/doi/abs/10.1029/2020JD033126](https://agupubs.onlinelibrary.wiley.com/doi/abs/10.1029/2020JD033126) (e2020JD033126 2020JD033126) doi:
 474 <https://doi.org/10.1029/2020JD033126>
- 475 Stock, M. G., Akita, M., Krehbiel, P. R., Rison, W., Edens, H. E., Kawasaki, Z., &
 476 Stanley, M. A. (2014). Continuous broadband digital interferometry of light-
 477 ning using a generalized cross-correlation algorithm. *Journal of Geophysical*
 478 *Research: Atmospheres*, *119*(6), 3134-3165. doi: 10.1002/2013JD020217
- 479 Thomas, R. J., Krehbiel, P. R., Rison, W., Hunyady, S. J., Winn, W. P., Hamlin,
 480 T., & Harlin, J. (2004). Accuracy of the lightning mapping array. *Journal of*
 481 *Geophysical Research: Atmospheres*, *109*(D14). doi: 10.1029/2004JD004549
- 482 van Haarlem, M. P., et al. (2013). LOFAR: The LOw-Frequency ARray. *A&A*, *556*,
 483 A2. doi: 10.1051/0004-6361/201220873